Microchimica Acta
https://doi.org/10.1007/s00604-017-2532-5

ORIGINAL PAPER

Electrochemical immunosensor for the breast cancer marker CA 15–3 based on the catalytic activity of a CuS/reduced graphene oxide nanocomposite towards the electrooxidation of catechol

Jafar Amani[1] · Alireza Khoshroo[1] · Mehdi Rahimi-Nasrabadi[2]

Received: 23 June 2017 / Accepted: 9 November 2017

Abstract
The authors report on an electrochemical immunosensor for the tumor marker carbohydrate antigen 15–3 (CA15–3). It is based on the use of a composite consisting of reduced graphene oxide (RGO) and copper sulfide (CuS) that was placed on a screen-printed graphite electrode. The electrode shows excellent activity towards the oxidation of catechol acting as an electrochemical probe, best at a working potential of 0.16 V. The electrode was modified with antibody against CA15–3. Once the analyte (CA15–3) binds to the surface of the electrode, the response to catechol is reduced. The assay has a linear response in the 1.0–150 U mL^{-1} CA15–3 concentration range, with a 0.3 U mL^{-1} lower detection limit and a sensitivity of 1.88 μA μM^{-1} cm^{-2}. The immunosensor also shows good reproducibility (2.7%), stability (95% of the initial values after storing for four weeks). The method was successfully applied to the determination of CA15–3 in serum samples, and results were found to compare well to those obtained by an ELISA. Conceivably, this nanocomposite based detection scheme has a wider scope and may be applied to numerous other immunoassays.

Keywords Screen-printed electrode · Copper sulfide · Carbohydrate antigen 15–3 · Tumor biomarkers · Immunosensors · Electrochemistry · Biosensor

Introduction

Carbohydrate antigen 15–3 (CA15–3) is a tumor marker that plays an important role in the diagnosis and screening for breast cancer. The serum CA15–3 level is below 30 U mL^{-1} for healthy individuals. Also, when the concentration of CA15–3 is over 100 U mL^{-1}, the patients can be considered to suffer from breast cancer [1]. The concentration of CA15–3 provides valuable information for monitoring the therapy. It can also early detection of recurrence of breast cancer after curative surgery [2]. Therefore, sensitive and selective determination of CA15–3 has a very important significance in clinical diagnoses. Some analytical methods, like chemiluminescence immunoassay [3], optical immunoassay [4], enzyme-linked immunosorption assay [5], sandwich-type immunosensor [6], have been developed for detection of CA15–3. However, these methods require complicated operations, expensive and complex equipment, and time-consuming pretreatment steps. Accordingly, electrochemical immunosensor has the advantages of high sensitivity, fast response, low cost and specific recognition and therefore, have been widely applied in the detection of tumor markers [7–10]. Ruo Yuan and coworkers constructed a mediator-less immunosensors based on the direct electrochemistry of glucose oxidase [11]. Wang et al. prepared a multi-labeled immunosensor for simultaneous detection of CA19–9 and CA15–3 [6]. Nonenzymatic electrochemical immunosensors improve the limited stability of the process. Enzyme is attached to a secondary antibody with a time-consuming, costly labeling process that often leads to denaturization of the biomolecules [12]. Qin Wei et al. constructed a FePt biosensor for the determination of CA15–3 on nonenzymatic immunosensor [13]. He Li et al. prepared a

✉ Mehdi Rahimi-Nasrabadi
rahiminasrabadi@gmail.com; rahimi@bmsu.ac.ir

[1] Applied Microbiology Research Center, System Biology and Poisonings Institute, Baqiyatallah University of Medical Sciences, Tehran, Iran

[2] Faculty of Pharmacy, Baqiyatallah University of Medical Sciences, Tehran, Iran

Published online: 26 December 2017

Cd^{2+}-functionalized nanoporous TiO_2 as labels for nonenzymatic determination of CA15–3 [14]. Turner et al. reported N-doped graphene sheets modified electrode for high sensitive determination of CA15–3 [15]. Among the above successful examples, lable-free immunosensor has drawn significant attention, which is based on the inhibiting the direct electron transfer generated from the redox probe to the electrode. This is due to the nonconductive immunocomplex from the specific immunological reaction [15].

Development of high sensitive and selective methods has become one of the most attractive topics in electrochemical sensors [16–20]. Many strategies based on nanomaterials have been applied in the electrochemical sensors due to the excellent performance [21]. To date, many nanomaterials have been widely used to develop immunosensor, owing to their perfect catalytic performance, such as carbon based nanomaterials [7], metal oxides nanoparticles [22], metal nitride nanoparticles [23] and noble metal nanoparticles [24].

Metal sulfides find extensive potential application in the field of signal amplification due to its catalytic activity [25–27]. Among these materials, copper sulfide enjoyed significant recent attention due to their excellent optical, electronic, physical and chemical properties which revealed potential application as catalysts in electrochemistry [28, 29].

To enhance the electrochemical performance, various strategies have been used to improve the catalytic activity of copper sulfide, such as employing carbon-based material as the support matrix [30, 31]. Graphene, a flat monolayer of carbon atoms tightly packed in to a 2D honeycomb lattice, is an excellent substrate for loading copper sulfide due to its excellent electronic conductivity, large surface area, good chemical stability and wide potential windows [32–35]. In this composite, reduced graphene oxide act as linker to improve the electrical connection between copper sulfides particles. Therefore, it is expected the reduced graphene oxide as anchoring matrix can enhance the electrochemical and catalytic performance of the copper sulfides. Based on these expectance, several papers shows intensive interests on the synthesis of copper sulfides with graphene composites for application in supercapacitor [36], lithium-ion batteries [31] and photocatalytic application [37].

Although several reports have been reported to the above applications, to the best of our knowledge, no study has been published so far reporting the copper sulfides with reduced graphene oxide (CuS-RGO) nanocomposites in immunosensor applications. Therefore, a novel electrochemical sensing platform for development of label free immunosensor for determination of CA15–3 biomarker was fabricated based on CuS-RGO nanocomposites (CuS-RGO) modified screen printed electrode (SPE). CuS-RGO nanocomposite shows excellent electrocatalytic activity towards catechol oxidation as probe in label free immunosensor. Therefore, quantitative detection of CA15–3 biomarker was successfully achieved. Because of the sensitive, reliable and specific nature of this method, the immunosensor can be extended to the detection of other biomarkers. In addition, immunosensors suffers greatly from stability. One of the most important components in biosensor is the bio-recognition molecule. Delicate handlings of antibodies are required to keep its reactivity such as low storage temperature, moisture control and light protection environment.

Experimental

Apparatus

Electrochemical data were collected with an Autolab potentiostat/galvanostat (PGSTAT-302 N, Eco Chemie, Netherlands, www.metrohm-autolab.com). The morphology of nanomaterial was characterized using scanning electron microscopy (SEM, Hitachi S-4160, www.hitachi-hightech.com) and transmission electron microscopy (TEM) (Philips EM208, www.philips.com). EIS measurements were carried out in the presence of 1.0 mM $[Fe(CN)_6]^{3-/4-}$ redox probe prepared in 0.1 M KCl, in a frequency range from 0.01 Hz to 100 kHz at a dc potential of 120 mV. Differential pulse voltammetry (DPV) was recorded within the potential range of 0.0 to 0.3 V under modulation amplitude of 50 mV (in 1.0 mM catechol prepared in 0.1 M phosphate buffer (pH 7.4)).

Materials and chemicals

Graphite powder, potassium chloride, catechol, phosphate salt, hydrochloric acid, sodium hydroxide, solvents and reagents were of pro-analysis grade from Merck (Darmstadt, Germany, www.merck.com). $CuSO_4.5H_2O$, thiourea and 1-pyrenebutyric acid N-hydroxysuccinimide ester (PANHS) were reagent grade from Sigma Aldrich (www.sigmaaldrich.com). CA15–3 antibody (Ab) and CA15–3 protein (Ag) were purchased from Abcam (Cambridge, UK, www.abcam.com).

Synthesis of the CuS-RGO nanocomposite

Graphene oxide (GO) was synthesized according to the modified Hummer's method [38]. In the synthesis of CuS-RGO, graphene oxide was dispersed in 40 mL deionized water via sonication for 2 h to form a homogeneous yellow-brown solution. $CuSO_4.5H_2O$ (1 mmol) and thiourea (2 mmol) was then added to the above suspension and was further sonicated for 60 min. The solution was transferred to a Teflon-lined autoclave and maintained at 180 °C for 24 h. The black precipitate was centrifuged and washed repeatedly with deionized water and alcohol to obtain composite. The product was dried at 60 °C for 24 h under vacuum.

Preparation of electrochemical immunosensor

First, 2 mg of CuS-RGO nanocomposite was dispersed in 1.0 mL ethanol by sonication for 1 h. 4 μL of nanocomposite suspension was coated onto the working electrode surface by micropipette and dried at room temperature to form a nanocomposite film at the working electrode and prepare a CuS-RGO–modified SPE (CuS-RGO/SPE). After, the electrodes were rinsed with deionized water.

Then 8 μL of PANHS solution (1 μmol L^{-1}) was dropped on the surface of modified electrode overnight in a saturated chamber with DMF vapor. For immobilization of anti-CA15–3 to the electrode surface, 8 μL of anti-CA15–3 solution (50 ppm) was pipetted on the modified electrode for 90 min at 4 °C and then washed with phosphate buffer (pH = 7.4) to remove unspecific physically adsorption. The remaining non-specific active sites on working electrode were blocked by ethanolamine solution (8 μL, 10 mM) for 30 min. The immunosensor (designed as CuS-RGO/Ab/SPE) was used for detection of CA15–3 biomarker during the experiment. The prepared immunosensor was stored at 4 °C for further use. The fabrication process of the electrochemical immunosensor is illustrated in Fig. 1.

Analytical procedure

For the determination of CA15–3 biomarker, the immunosensor (CuS-RGO/Ab/SPE) incubated with a different concentration of CA15–3 for 3 h at 4 °C, and subsequently the immunosensor was rinsed with water to eliminate possible unstable adsorbed CA15–3 from the electrode surface. Electrochemical measurements of this immunosensor toward CA15–3 samples were carried out by 1.0 mM catechol in 0.1 M phosphate buffer (pH = 7.4). After adding CA15–3 antigen, it will form complexes with antibody; therefore, covered the surface of CuS-RGO/Ab/SPE and blocked the catalysis effect of CuS-RGO to the oxidation of catechol. The current response in differential pulse voltammetry (DPV) decreased with the increase of CA15–3 concentration. The decrease of DPV peak current is proportion to the increasing concentrations of CA15–3, which will use to determination of CA15–3.

Results and discussion

Characterization of the nanocomposite

SEM and TEM was used to characterize the structure and morphology of the CuS-RGO nanocomposite. Fig. 2a, b clearly shows the product contains CuS nanoparticles uniformly are decorated on the surface of the RGO nanosheet, evidencing the successful formation of composite. This can be attributed to oxygen-containing functional groups such as hydroxyl, epoxide and carboxylic groups uniformly distributed on the RGO sheets. Those oxygen-containing groups on the sheets provide multiple binding sites for the reaction between Cu^{2+} ions and GO and inhibited aggregation. When RGO was absence, CuS nanoparticles (Fig. 2c) were severely agglomerated. This is due to the fact that the large surface-to-volume

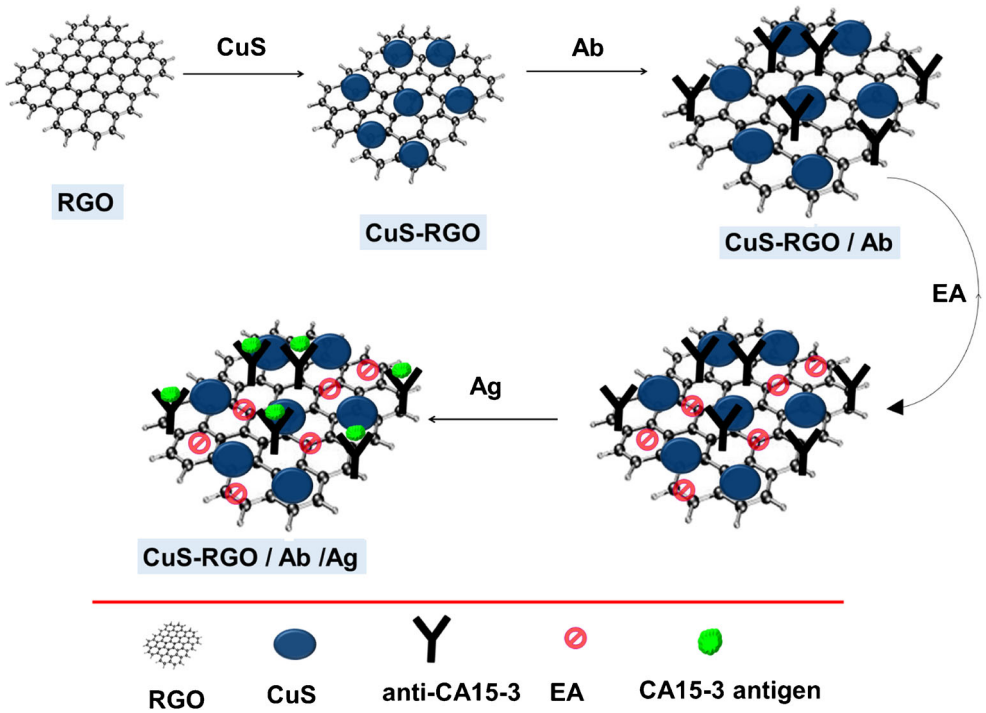

Fig. 1 Schematic exhibition of fabrication process of the immunosensor

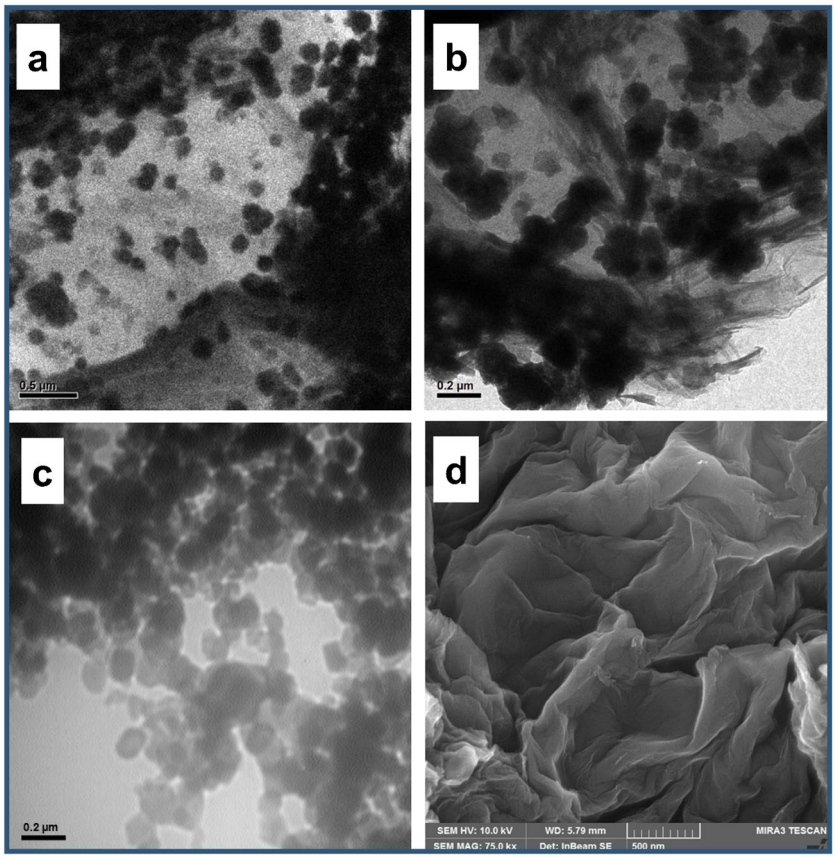

Fig. 2 TEM image of CuS-RGO nanocomposite (**a**, **b**) and CuS particle (**c**). **d** SEM image of RGO

ratio of CuS nanoparticles, which lead them to tend to self-agglomerate during their re-dispersion in water. Such differences suggested that CuS nanoparticles supported on RGO sheets possessed a much better dispersibility, which would yield better catalytic activity. As shown in Fig. 2d, the RGO exhibited a morphology consisting of a thin wrinkling paper-like structure. In addition, for preparation of TEM specimen, resulting CuS-RGO composite added into alcohol and subjected the suspension to ultrasonication, but the CuS nanoparticles are still well dispersed on RGO, indicating the strong interaction between CuS nanoparticles and RGO.

The electrochemical characterization of the modified electrodes

A label-free immunosensor for the detection of CA15–3 antigen was prepared by modified SPE with the CuS-RGO nanocomposite. CuS-RGO offers numerous possibilities for coupling of antibody under reaction conditions. The antibody-coated electrode then was used to capture CA15–3 from the CA15–3-containing solution. This assay was characterized by cyclic voltammetry (CV) and electrochemical impedance spectroscopy EIS.

CV was used for investigated the electrocatalytic activity of the CuS-RGO modified SPE toward oxidation of catechol (Fig. 3a). A pair of well-defined redox peaks is observed at the bare SPE (Fig. 3a, curve a). After modified of bare SPE, the peak current increased obviously (curve c) due to the electrocatalytic effect of CuS-RGO for oxidation of catechol (peak potential: 0.15 V), This can be ascribed to the fact that CuS-RGO can significantly enhance the effective surface area and facilitate the electron transfer. To investigate the roles of CuS in CuS-RGO nanocomposite in the peak current, the CVs of catechol at the CuS-RGO/SPE (curve c) and RGO/SPE (curve b) were recorded. The results indicated that the presence of CuS on the RGO sheets improved the oxidation peak current for catechol. The excellent physical and chemical properties of RGO and the unique properties of CuS were helpful for promoting the electrochemical response. When anti-CA15–3 was induced onto the surface of the electrode (curve b, Fig. 3b), the peak current decreased. This is due to the formation of insulating layers of proteins, perturbs the interfacial electron transfer considerably and prevents the electrocatalytic oxidation of catechol. Subsequently, when non-electroactive ethanolamine was used to block nonspecific sites, the peak current further decreased (curve c, Fig. 3b). After CA15–3 antigen was immobilized on the electrode, there is another decrease of peak current (curve d, Fig. 4b). This can be attributed to the formation of immunocomplexes between antibody and antigen acted as the electron-transfer insulating layer, which

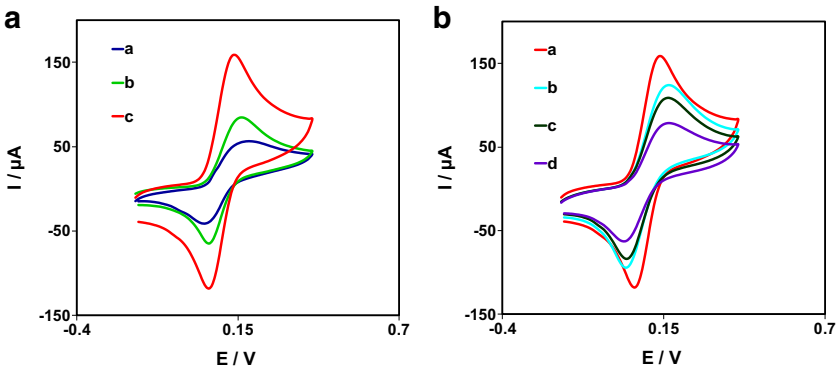

Fig. 3 **a** Cyclic voltammograms of bare SPE (a), RGO/SPE (b) and CuS-RGO/SPE (c) in phosphate buffer (pH = 7.4) containing 1.0 mM catechol. **b** Cyclic voltammograms of CuS-RGO/SPE (a), CuS-RGO/Ab/SPE (b) and CuS-RGO/Ab/Ag/SPE (c) in phosphate buffer (pH = 7.4) containing 1.0 mM catechol

perturbed the reaction of catechol on the electrode surface. Therefore, this change in the CVs during the fabrication process of the immunosensor, indicates an efficient bonding of them over the CuS-RGO surface.

In order to further investigate the assembly process of the immunosensor, EIS techniques were also employed. Fig. 4a shows the impedance spectra demonstrate as Nyquist plots for bare SPE (a), RGO/SPE (b) and CuS-RGO/SPE (c) in 1.0 mM $Fe(CN)_6^{3-/4-}$ containing 0.1 M KCl solution. The semicircle diameter in the impedance spectrum equals to the charge-transfer resistance (R_{ct}). It can be seen that on the CuS-RGO/SPE (curve c, R_{ct} = 42 kΩ) the value of R_{ct} is smaller than to RGO/SPE (curve b, R_{ct} = 216 kΩ) and bare SPE (curve a, R_{ct} = 270 kΩ). This is due to the excellent electrical property of CuS-RGO nanocomposite that formed a high electron conduction pathway between the electrode and electroactive indicator. Subsequently, when the antibody, CA15–3, was conjugated onto CuS-RGO/SPE surface, the resistance was increased (Fig. 4a, curve b, R_{ct} = 130 kΩ), suggesting that anti-CA15–3 was successfully immobilized on the surface of the electrode and generated a barrier for electron-transfer. Similarly, R_{ct} further increased with the assembled of CA15–3 antigen (curve c, R_{ct} = 220 kΩ) on the immunosensor above, because the formed antigen–antibody complex between the antigens and the antibodies on the CuS-RGO/Ab/SPE serve as an insulated layer, and perturbed the electron transfer. The result indicated that the hydrophobic layer of the protein (antibody and antigen) on the modified electrode generated a barrier for electron-transfer, which was similar to the previous report [39]. The changes of the charge-transfer resistance (R_{ct}) during the fabrication process of the immunosensor are another convincing proof for the successful fabrication of this immunosensor.

Optimization of experimental conditions

In order to achieve better experimental results, the experimental conditions need to be optimized, including the antibody concentration, incubation time of anti-CA15–3 and incubation time of antigen [40–44]. The effect of the incubation time of anti-CA15–3 time was studied. Based on the results, with the increasing the incubation time of antibody from 30 to 180 min, R_{ct} increased and then decreased (Fig. 5a), with the maximum R_{ct} at 90 min. This may be due to the full coverage of the electrode surface by the anti-CA15–3 after 90 min. Therefore, an incubation time of 90 min was selected for subsequent studies. In immunosensors, increasing the immobilization

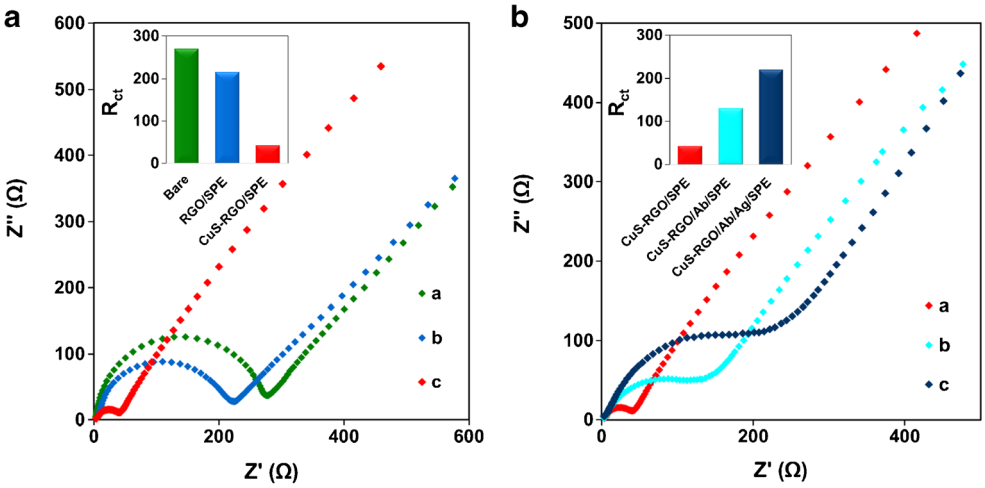

Fig. 4 **a** Nyquist plots of bare SPE (a), RGO/SPE (b) and CuS-RGO/SPE (c) in 0.1 M KCl and 1.0 mM $[Fe(CN)_6]^{3-/4-}$. **b** Nyquist plots of CuS-RGO/SPE (a), CuS-RGO/Ab/SPE (b) and CuS-RGO/Ab/Ag/SPE (c) in 0.1 M KCl and 1.0 mM $[Fe(CN)_6]^{3-/4}$

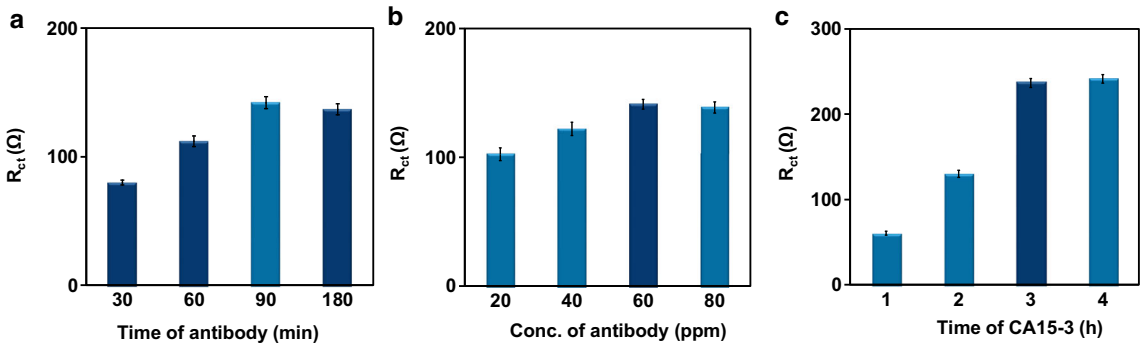

Fig. 5 Optimization of: **a** incubation time and (**b**) the concentration of antibody, (**c**) incubation time of CA15–3 antigen. EIS responses were performed in 0.1 M KCl and 1.0 mM $[Fe(CN)_6]^{3-/4-}$

amount of antibodies would markedly enhance the detection ability of sensor. Therefore, different concentrations of anti-CA15–3 solution (20, 40, 60 and 80 ppm) were used to optimize the anti-CA15–3 concentration (Fig. 5b). With increasing anti-CA15–3 concentration, the response increased gradually up to 60 ppm and then reached a constant level. Therefore, 60 ppm was used for the concentration of CA153 in this study. Similarly, the effect of the incubation times of CA15–3 antigen on sensitivity of immunosensor were also investigated and optimum times of 3 h was adopted (Fig. 5c).

Performance of the immunosensor

Under optimum conditions, DPV techniques were applied for determination of different CA15–3 antigen concentrations by fabricated immunosensor. With increasing concentrations of CA15–3 antigen, DPV responses decreased due to formation of immunocomplexes between antibody and antigen (Fig. 6). These observations represent less electron transfer following CA15–3 antigen captured by immunosensor. This is due to the above mentioned facts: the insulating protein CA15–3 antigen blocked the interfacial electron transfer considerably and prevents the electrocatalytic oxidation of probe and thereby resulted in the decrease of DPV current. The immunosensor exhibited a good linear relationship with the CA15–3 antigen concentration from 1.0 to 150.0 U mL^{-1}. The detection limit (LOD) for the CA15–3 antigen based on $3s_b/m$ (where s_b is the standard deviation of a blank solution and m is the slope of the calibration curve) was estimated to be 0.3 U mL^{-1}. The results indicate that the linear range (1.0–150.0 U mL^{-1}), detection limit (0.3 U mL^{-1}) and sensitivity of 1.88 μA μM^{-1} cm^{-2} obtained in this work are suitable for detection of CA15–3 antigen. The results of the immunosensor are comparable with other CA15–3 sensors that were displayed in Table 1. This confirms that the presented immunosensor shows better analytical performances to than other techniques [4, 6, 11, 45–47].

Recognition of differences between the targets antigen from others is obviously an important factor to check it for the immunoassay method. So, the specificity of the immunosensor was investigated by using CEA, BSA and TNF-α antigens (inset of Fig. 6). The immunosensors were separately incubated in two kinds of 25 U mL^{-1} CA15–3 antigen incubating solution: one solution with the interferent and the other without. These results showed that the immunosensor satisfied selectivity for CA15–3 antigen under the experimental conditions.

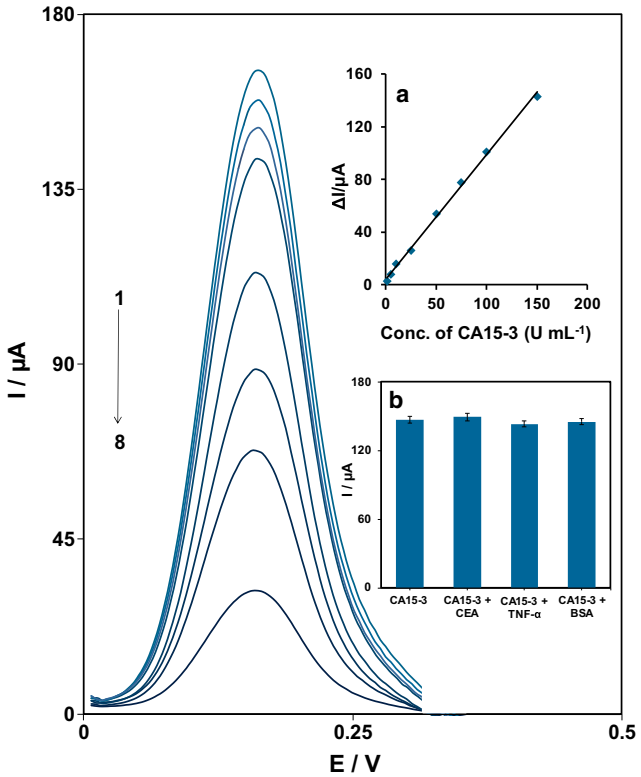

Fig. 6 DPV responses of the immunosensor to 1.0 mM catechol in phosphate buffer (pH = 7.4) at different concentrations of CA15–3 antigen. The numbers of 1–8 correspond to: 150.0, 100.0, 75.0, 50.0, 25.0, 10.0, 5.0, and 1.0 U mL^{-1}, respectively. The inset is the calibration curve (data obtained at the E = 0.17 V)

Table 1 A comparison of the performance of several immunosensors for the detection of CA15–3

Detection methods	Material	Linear range (U mL^{-1})	Detection limit (U mL^{-1})	Reproducibility (%)	Ref.
Electrochemiluminescence	ZnO porous	0.05–120	0.014	3.9	[4]
Electrochemical immunoassay	TiO_2 nanoparticles	1–100	0.3	1.1–2.2	[6]
Surface plasmon resonance	gold/zinc oxide	1–40	0.025	–	[45]
The kinetic-exclusion analytical technology	Polymethylmethacrylate	0.3–20	0.21	5.2–7.4	[46]
Sandwich-type electrochemical immunosensors	IL functionalized reduced graphene oxide	0.02–60	0.008	3.9	[14]
Non enzymatic immunosensor	nanoporous PtFe alloy	0.002–40	3×10^{-4}	2.3–3.7	[13]
Enzyme-linked immunosensor	Organosilica @ chitosan	0.1–160	0.04	5.4–6.7	[11]
Scanning electrochemical microscopy	horseradish peroxidase	15–250	2.5	–	[47]
Enzyme-free electrochemical immunosensor	CuS-RGO nanocomposite	0.1–150	0.03	2.4–2.7	This work

Stability and reproducibility of the immunosensor

Stability plays a crucial role in their application and development of the immunosensor for the detection of CA15–3. Therefore, the storage stability of the immunoassay system was examined. When the immunosensor was stored at 4 °C in refrigerator, it retained more than about 95% of the initial values after storing for four weeks, which indicated that the immunosensor had acceptable stability. The reason might be the fact that the CuS-RGO nanocomposite provided a favorable microenvironment for anti-CA15–3 biomolecules on the surface. To evaluate the fabrication reproducibility of this immunosensor, a series of seven different modified electrodes were used for the detection of same concentration of CA15–3 antigen. The RSD of the measurements were 2.9%, 2.6%, 2.4% and 2.7% for the detection of 130, 50, 20 U mL^{-1} and 10 U mL^{-1} of CA15–3 antigen, respectively, which suggested that the reproducibility of the immunosensor was acceptable.

Application of the immunosensor in human serum

In order to assess the analytical application of this method for clinical diagnosis, the detection of CA15–3 antigen in the human serum samples (obtained from local hospital) was performed. The serum samples were diluted 10-fold with phosphate buffer (pH 7.4). The CA15–3 antigen contents of these samples were assayed using the immunosensor and the ELISA method as the referenced method. Statistical comparison of the experimental results is summarized in Table 2. As seen, the results by the immunosensor are in satisfactory agreement, within the experimental errors presented, with those reported using the corresponding commercially available ELISA Kit. t tests indicated no significant differences between the immunosensor and the commercial ELISA method at a confidence level of 95% ($t_{calculated} < t_{theoretical}$). This result implied that the immunosensor was a potential tool for the analytical application in clinical analysis.

Conclusions

In this work, a label-free electrochemical immunosensor was constructed for determination of CA15–3 antigen based on CuS-RGO nanocomposites as the efficient platform and electrocatalyst. The immunosensor presented some advantages, including a rapid method for protein detection, avoided the need of enzyme, good selectivity, sensitive, wide linear range and low detection limit, satisfactory reproducibility and stability. The determination of CA15–3 in human serum samples with satisfactory results was obtained. CuS-RGO

Table 2 CA15–3 concentration (U mL^{-1}) in human serum samples obtained by the immunosensor and ELISA method

Serum sample no.	Immunosensor, (n = 3)	ELISA method ($n = 3$)	Relative error (%)	t-test
1	38.2 ± 0.4	37.1 ± 0.3	3.0	3.8
2	40.3 ± 0.5	38.9 ± 0.6	3.6	2.6
3	48.6 ± 0.6	49.7 ± 0.8	−2.2	1.9
4	99.4 ± 0.9	98.0 ± 0.7	1.4	2.1
5	121.1 ± 0.8	123.2 ± 0.9	1.7	3.0

[a] Tabulated t-values, at $P = 0.05$, are 4.3

nanocomposites can be anchored with various antibodies, so this immunosensor holds great potential for detection of all other biomarkers in clinical diagnostics.

Acknowledgements The authors wish to thank the National Institute for Medical Research Development (NIMAD) for their support (Grant No. 957254).

Compliance with ethical standards The authors declare that they have no competing interests.

References

1. Wu J, Fu Z, Yan F, Ju H (2007) Biomedical and clinical applications of immunoassays and immunosensors for tumor markers. TrAC Trends Anal Chem 26:679–688
2. Müller V, Stahmann N, Riethdorf S et al (2005) Circulating tumor cells in breast cancer: correlation to bone marrow micrometastases, heterogeneous response to systemic therapy and low proliferative activity. Clin Cancer Res 11:3678–3685
3. Liu A, Zhao F, Zhao Y et al (2016) A portable chemiluminescence imaging immunoassay for simultaneous detection of different isoforms of prostate specific antigen in serum. Biosens Bioelectron 81: 97–102
4. Zhang L, He Y, Wang H et al (2015) A self-enhanced electrochemiluminescence immunosensor based on l-Lys-Ru functionalized porous six arrises column nanorods for detection of CA15-3. Biosens Bioelectron 74:924–930
5. Ambrosi A, Airo F, Merkoçi A (2009) Enhanced gold nanoparticle based ELISA for a breast cancer biomarker. Anal Chem 82:1151–1156
6. Wang G, Qing Y, Shan J et al (2013) Cation-exchange antibody labeling for simultaneous electrochemical detection of tumor markers CA15-3 and CA19-9. Microchim Acta 180:651–657
7. Mazloum-Ardakani M, Hosseinzadeh L, Khoshroo A (2015) Ultrasensitive electrochemical Immunosensor for detection of tumor necrosis factor-α based on functionalized MWCNT-gold nanoparticle/ionic liquid nanocomposite. Electroanalysis 27: 2518–2526
8. Zhang A, Huang C, Shi H et al (2017) Electrochemiluminescence immunosensor for sensitive determination of tumor biomarker CEA based on multifunctionalized flower-like Au@ BSA nanoparticles. Sensors Actuators B Chem 238:24–31
9. Mazloum-Ardakani M, Hosseinzadeh L, Khoshroo A (2015) Label-free electrochemical immunosensor for detection of tumor necrosis factor α based on fullerene-functionalized carbon nanotubes/ionic liquid. J Electroanal Chem 757:58–64
10. Roushani M, Valipour A (2016) Voltammetric immunosensor for human chorionic gonadotropin using a glassy carbon electrode modified with silver nanoparticles and a nanocomposite composed of graphene, chitosan and ionic liquid, and using riboflavin as a redox probe. Microchim Acta 183:845–853
11. Li W, Yuan R, Chai Y, Chen S (2010) Reagentless amperometric cancer antigen 15-3 immunosensor based on enzyme-mediated direct electrochemistry. Biosens Bioelectron 25:2548–2552
12. Kurtinaitiene B, Ambrozaite D, Laurinavicius V et al (2008) Amperometric immunosensor for diagnosis of BLV infection. Biosens Bioelectron 23:1547–1554
13. Li Y, Xu C, Li H et al (2014) Nonenzymatic immunosensor for detection of carbohydrate antigen 15-3 based on hierarchical nanoporous PtFe alloy. Biosens Bioelectron 56:295–299
14. Zhao L, Wei Q, Wu H et al (2014) Ionic liquid functionalized graphene based immunosensor for sensitive detection of carbohydrate antigen 15-3 integrated with Cd^{2+}-functionalized nanoporous TiO_2 as labels. Biosens Bioelectron 59:75–80
15. Li H, He J, Li S, Turner APF (2013) Electrochemical immunosensor with N-doped graphene-modified electrode for label-free detection of the breast cancer biomarker CA 15-3. Biosens Bioelectron 43:25–29
16. Hosseinzadeh L, Abassi S, Ahmadi F (2007) Adsorptive cathodic stripping voltammetry determination of ultra trace of lead in different real samples. Anal Lett 40:2693–2707
17. Ganjali MR, Rahimi-Nasrabadi M, Maddah B et al (2004) Submicro level monitoring of beryllium ions with a novel beryllium sensor based on 2, 6-diphenyl-4-benzo-9-crown-3-pyridine. Talanta 63:899–906
18. Ganjali MR, Gholivand MB, Rahimi-Nasrabadi M, Maddah B, Salavati-Niasari M, Ahmadi F (2006) Synthesis of a new octadentates Schiff's base and its application in construction of a highly selective and sensitive lanthanum (III) membrane sensor. Sens Lett 4:356–363
19. Shan J, Ma Z (2017) A review on amperometric immunoassays for tumor markers based on the use of hybrid materials consisting of conducting polymers and noble metal nanomaterials. Microchim Acta 148:969–979
20. Gao Z, Lin Y, He Y, Tang D (2017) Enzyme-free amperometric glucose sensor using a glassy carbon electrode modified with poly(-vinyl butyral) incorporating a hybrid nanostructure composed of molybdenum disulfide and copper sulfide. Microchim Acta 184: 807–814
21. Rahimi-Nasrabadi M, Khoshroo A, Mazloum-Ardakani M (2017) Electrochemical determination of diazepam in real samples based on fullerene-functionalized carbon nanotubes/ionic liquid nanocomposite. Sensors Actuators B Chem 240:125–131
22. Pandey CM, Tiwari I, Singh VN et al (2017) Highly sensitive electrochemical immunosensor based on graphene-wrapped copper oxide-cysteine hierarchical structure for detection of pathogenic bacteria. Sensors Actuators B Chem 238:1060–1069
23. Ali MA, Mondal K, Wang Y et al (2017) In situ integration of graphene foam–titanium nitride based bio-scaffolds and microfluidic structures for soil nutrient sensors. Lab Chip 17:247–285
24. Liu N, Nie D, Tan Y et al (2017) An ultrasensitive amperometric immunosensor for zearalenones based on oriented antibody immobilization on a glassy carbon electrode modified with MWCNTs and AuPt nanoparticles. Microchim Acta 184:147–153
25. Xie X, Ao Z, Su D et al (2015) MoS_2/graphene composite anodes with enhanced performance for sodium-ion batteries: the role of the two-dimensional Heterointerface. Adv Funct Mater 25:1393–1403
26. Tang D, Hou L, Niessner R et al (2013) Multiplexed electrochemical immunoassay of biomarkers using metal sulfide quantum dot nanolabels and trifunctionalized magnetic beads. Biosens Bioelectron 46:37–43
27. Pourmortazavi SM, Hajimirsadeghi SS, Rahimi-Nasrabadi M (2009) Statistical optimization of condition for synthesis lead sulfide nanoparticles. Mater Manuf Process 24:524–528
28. Yu X, Cao C, Zhu H et al (2007) Nanometer-sized copper sulfide hollow spheres with strong optical-limiting properties. Adv Funct Mater 17:1397–1401
29. Xie Y, Carbone L, Nobile C et al (2013) Metallic-like stoichiometric copper sulfide nanocrystals: phase-and shape-selective synthesis, near-infrared surface plasmon resonance properties, and their modeling. ACS Nano 7:7352–7369
30. Lee H, Yoon SW, Kim EJ, Park J (2007) In-situ growth of copper sulfide nanocrystals on multiwalled carbon nanotubes and their application as novel solar cell and amperometric glucose sensor materials. Nano Lett 7:778–784

31. Feng C, Zhang L, Yang M et al (2015) One-pot synthesis of copper sulfide nanowires/reduced graphene oxide nanocomposites with excellent lithium-storage properties as anode materials for lithium-ion batteries. ACS Appl Mater Interfaces 7:15726–15734
32. Huang X, Yin Z, Wu S et al (2011) Graphene-based materials: synthesis, characterization, properties, and applications. Small 7: 1876–1902
33. Geim AK (2009) Graphene: status and prospects. Science 324: 1530–1534
34. Rahimi-Nasrabadi M, Rostami M, Ahmadi F et al (2016) Synthesis and characterization of $ZnFe_2-xYbxO_4$–graphene nanocomposites by sol–gel method. J Mater Sci Mater Electron 27:11940–11945
35. Rostami M, Rahimi-Nasrabadi M, Ganjali MR et al (2017) Facile synthesis and characterization of TiO_2–graphene–$ZnFe_2-xTbxO_4$ ternary nano-hybrids. J Mater Sci 52:7008–7016
36. Huang K-J, Zhang J-Z, Liu Y, Liu Y-M (2015) Synthesis of reduced graphene oxide wrapped-copper sulfide hollow spheres as electrode material for supercapacitor. Int J Hydrog Energy 40:10158–10167
37. Zhang Y, Tian J, Li H et al (2012) Biomolecule-assisted, environmentally friendly, one-pot synthesis of CuS/reduced graphene oxide nanocomposites with enhanced photocatalytic performance. Langmuir 28:12893–12900
38. Marcano DC, Kosynkin DV, Berlin JM et al (2010) Improved synthesis of graphene oxide. ACS Nano 4:4806–4814
39. Mazloum-Ardakani M, Hosseinzadeh L, Taleat Z (2014) Two kinds of electrochemical immunoassays for the tumor necrosis factor α in human serum using screen-printed graphite electrodes modified with poly(anthranilic acid). Microchim Acta 181:917–924
40. Yannopoulos SI, Lyberatos G, Theodossiou N et al (2015) Evolution of water lifting devices (pumps) over the centuries worldwide. Water 7:5031–5060
41. Valipour M (2016) Optimization of neural networks for precipitation analysis in a humid region to detect drought and wet year alarms. Meteorol Appl 23:91–100
42. Valipour M (2015) Study of different climatic conditions to assess the role of solar radiation in reference crop evapotranspiration equations. Arch Agron Soil Sci 61:679–694
43. Valipour M (2012) Number of required observation data for rainfall forecasting according to the climate conditions. Am J Sci Res 74: 79–86
44. Valipour M (2013) Increasing irrigation efficiency by management strategies: cutback and surge irrigation. ARPN J Agric Biol Sci 8: 35–43
45. Chang C-C, Chiu N-F, Lin DS et al (2010) High-sensitivity detection of carbohydrate antigen 15-3 using a gold/zinc oxide thin film surface plasmon resonance-based biosensor. Anal Chem 82:1207–1212
46. Darwish IA, Wani TA, Khalil NY, Blake DA (2012) Novel automated flow-based immunosensor for real-time measurement of the breast cancer biomarker CA15-3 in serum. Talanta 97:499–504
47. Zhang X, Peng X, Jin W (2006) Scanning electrochemical microscopy with enzyme immunoassay of the cancer-related antigen CA15-3. Anal Chim Acta 558:110–114